JEM Journal of Experimental Medicine

ARTICLE

PTEN deletion in luminal cells of mature prostate induces replication stress and senescence in vivo

Maxime Parisotto, Elise Grelet*, Rana El Bizri*, Yongyuan Dai, Julie Terzic, Doriane Eckert, Laetitia Gargowitsch, Jean-Marc Bornert, and Daniel Metzger

Genetic ablation of the tumor suppressor *PTEN* in prostatic epithelial cells (PECs) induces cell senescence. However, unlike oncogene-induced senescence, no hyperproliferation phase and no signs of DNA damage response (DDR) were observed in *PTEN*-deficient PECs; *PTEN* loss-induced senescence (PICS) was reported to be a novel type of cellular senescence. Our study reveals that *PTEN* ablation in prostatic luminal epithelial cells of adult mice stimulates PEC proliferation, followed by a progressive growth arrest with characteristics of cell senescence. Importantly, we also show that proliferating *PTEN*-deficient PECs undergo replication stress and mount a DDR leading to p53 stabilization, which is however delayed by Mdm2-mediated p53 down-regulation. Thus, even though *PTEN*-deficiency induces cellular senescence that restrains tumor progression, as it involves replication stress, strategies promoting *PTEN* loss–induced senescence are at risk for cancer prevention and therapy.

Introduction

Mutations or deletion of the *PTEN* locus are common and associated with metastasis and resistance to therapeutic castration in prostate cancer (Cairns et al., 1997; Choucair et al., 2012; Krohn et al., 2012; Costa et al., 2015). Genetic ablation of *PTEN* or expression of a dominant-negative mutant of PTEN in mouse prostate epithelial cells (PECs) induces prostatic intraepithelial neoplasia (PIN) with full penetrance (Chen et al., 2005; Luchman et al., 2008; Ratnacaram et al., 2008; Papa et al., 2014).

Several studies have shown that the progression of *PTEN* loss–induced PINs is antagonized by cell senescence in mice (Chen et al., 2005; Alimonti et al., 2010; Di Mitri et al., 2014). Senescence is triggered in response to various stimuli (Yaswen and Campisi, 2007; Courtois-Cox et al., 2008), including the expression of oncogenes in untransformed cells (e.g., Ras^{G12V}, E2F1, Raf, Mos, Cdc6, cyclin E, Stat5, and PML; Serrano et al., 1997; Ferbeyre et al., 2000; Michaloglou et al., 2005; Mallette et al., 2007; Courtois-Cox et al., 2008). Oncogene-induced senescence (OIS), by permanently halting cell proliferation and promoting immune surveillance of premalignant lesions, is a barrier against cell transformation (Braig et al., 2005; Chen et al., 2005; Kang et al., 2011). Accordingly, markers of senescence have been observed in premalignant lesions in various human tissues, including the prostate, but not in the corresponding tumors (Chen et al., 2005; Michaloglou et al., 2005; Collado and Serrano, 2010; Vernier et al., 2011). Thus, escaping or avoiding OIS likely represents a critical step toward transformation.

The DNA damage response (DDR) pathway is a central regulator of OIS (Bartkova et al., 2006; Bartek et al., 2007; Mallette et al., 2007; Courtois-Cox et al., 2008). Indeed, the expression of oncogenes has been shown to stimulate cell proliferation, causing replication stress and a robust activation of the DDR pathway (Bartkova et al., 2006; Bartek et al., 2007), whereas inactivation of components of the DDR pathway bypasses OIS (Di Micco et al., 2006; Mallette et al., 2007). Induction of the DDR stabilizes p53 through its phosphorylation by DDR kinases (ATR, ATM, DNA-PK, CHK1, and CHK2; Zhou and Elledge, 2000; Lavin and Gueven, 2006). p53 promotes OIS through transcriptional regulation of an array of genes, including p21, an inhibitor of cell cycle progression (Mirzayans et al., 2012).

PTEN loss–induced senescence (PICS) was also shown to be p53-dependent (Chen et al., 2005), but as no hyperproliferation and DDR activation was observed (Alimonti et al., 2010; Astle et al., 2012), it was concluded that PICS is a new type of senescence (Chen et al., 2005; Courtois-Cox et al., 2008; Astle et al., 2012). Moreover, Di Mitri et al. reported that tumor-infiltrated GR-1–positive myeloid cells antagonize PICS and sustain tumor growth (Di Mitri et al., 2014).

Department of Functional Genomics and Cancer, Institut de Génétique et de Biologie Moléculaire et Cellulaire (IGBMC), Centre National de la Recherche Scientifique UMR7104/Institut National de la Santé et de la Recherche Médicale U1258, Université de Strasbourg, Illkirch Cedex, France.

*E. Grelet and R. El Bizri contributed equally to this paper; Correspondence to Daniel Metzger: metzger@igbmc.fr; M. Parisotto's current address is Université de Montréal, Montréal, Québec, Canada.

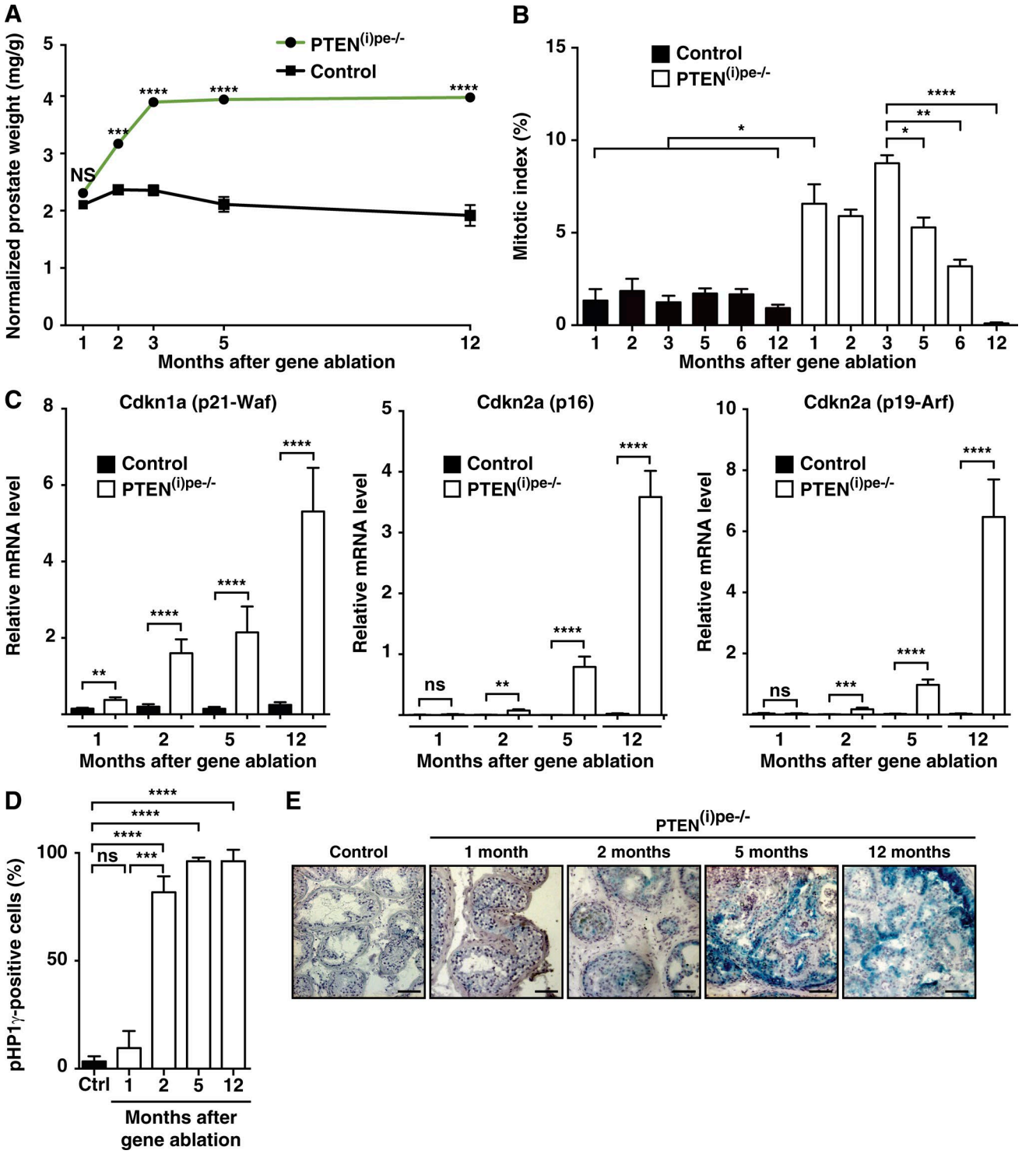

Figure 1. **Characterization of prostate tumors in PTEN$^{(i)pe-/-}$ mice. (A)** Prostate weight (normalized over body weight) in PTEN$^{(i)pe-/-}$ and control mice over 12 mo after *PTEN* ablation. Values are mean of four to six mice ± SEM. **(B)** Proliferation index (percentage of Ki67-positive epithelial cells) of DLP in PTEN$^{(i)pe-/-}$ and control mice over 12 mo after gene ablation. Values are mean of four to eight mice ± SEM. Data are representative of two experiments. **(C)** Relative transcript levels of *Cdkn1a* (*p21*) and *Cdkn2a* (*p16* and *p19ARF*) in the prostate of PTEN$^{(i)pe-/-}$ and control mice over 12 mo after gene ablation. Values are mean from four to eight mice ± SEM. **(D)** Quantification of pHP1γ-positive cells in DLP epithelium of PTEN$^{(i)pe-/-}$ and control mice over 12 mo after gene ablation. Values are mean from four to six mice ± SEM. **(E)** Representative SA-βGal staining (blue) of DLP sections of PTEN$^{(i)pe-/-}$ and control mice sacrificed at indicated time points after gene ablation. Pink, hematoxylin staining. Bars, 250 µm. Four to six mice were analyzed for each time point. ns, not significant, P value ≥ 0.05; *, P value < 0.05; **, P value < 0.01; ***, P value < 0.001; ****, P value < 0.0001.

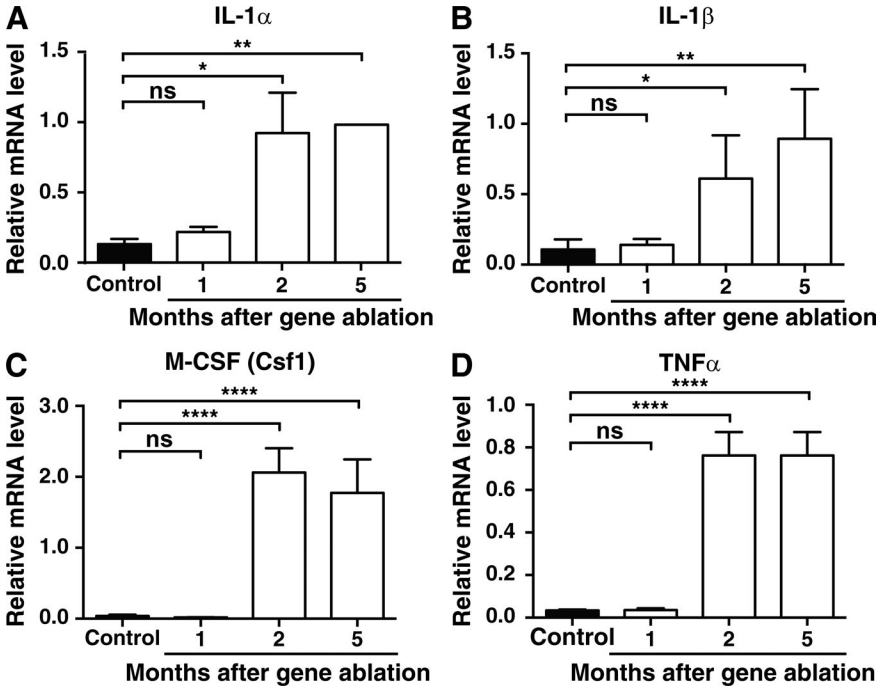

Figure 2. **Characterization of the senescence-associated secretory phenotype in the prostate of PTEN$^{(i)pe-/-}$ mice. (A–D)** Relative transcript levels of *Il-1α* (A), *Il-1β* (B), *M-CSF* (C), and *TNFα* (D) in the prostate of PTEN$^{(i)pe-/-}$ and control mice over 5 mo after gene ablation. Values are mean of four to six mice ± SEM. Data are representative of three experiments. ns, not significant. *, P value < 0.05; **, P value < 0.01; ****, P value < 0.0001.

To further characterize PICS in vivo, we analyzed PTEN$^{(i)pe-/-}$ mice in which *PTEN* is selectively ablated in prostatic luminal cells at adulthood, via the tamoxifen (Tam)-dependent Cre-ER^{T2} system (Ratnacaram et al., 2008). These mice develop slowly progressing PIN lesions with a highly reproducible kinetics. We took advantage of the strict temporal control of *PTEN* ablation in this model to characterize the fate of *PTEN*-deficient PECs. Our study reveals that *PTEN* ablation stimulates proliferation of PECs during several months, followed by a progressive growth arrest with characteristics of cell senescence. Importantly, we also show that proliferating *PTEN*-deficient PECs undergo replication stress and mount a DDR that stabilizes p53. However, as p53 is actively down-regulated at early time by Mdm2, cell senescence is delayed by several months.

Results

PTEN-deficient PECs actively proliferate to generate PINs prior to becoming senescent

To study the consequences of *PTEN* loss in PECs of adult mice, we analyzed PTEN$^{(i)pe-/-}$ and PTEN$^{pe+/+}$ (control) mice over a period of 12 mo after *PTEN* ablation (Fig. S1 A). The prostate weight of PTEN$^{(i)pe-/-}$ mice increased during the first 3 mo after *PTEN* ablation to reach twice that of control mice and remained stable for the following 9 mo (Fig. 1 A). In agreement with previous results (Ratnacaram et al., 2008), the levels of pAKT S473 were enhanced in the prostate of PTEN$^{(i)pe-/-}$ mice, and >75% of the glands in the dorsolateral prostate (DLP) contained PINs between 1 and 12 mo (Fig. S1, B–E). The mitotic index of PECs was approximately four- to fivefold higher in PTEN$^{(i)pe-/-}$ mice than in control mice between 1 and 3 mo, but progressively decreased at a later time (Fig. 1 B). No terminal deoxynucleotidyl transferase dUTP nick end labeling (TUNEL)-positive apoptotic cells were observed in PECs of PTEN$^{(i)pe-/-}$ mice (Fig. S1 F), but transcript levels of the negative regulators of cell cycle progression *Cdkn1a* (*p21*) and *Cdkn2a* (*p16* and *p19ARF*) were markedly increased at 5 mo and 12 mo (Fig. 1 C). In contrast, transcript levels of *p16* and *p19ARF* were similar in PTEN$^{(i)pe-/-}$ and control mice at 1 mo and slightly increased at 2 mo, whereas those of *p21* were increased by 2-fold at 1 mo and by 10-fold at 2 mo (Fig. 1 C). From 2 to 12 mo, >95% PIN cells in DLP of PTEN$^{(i)pe-/-}$ mice displayed nuclear foci of phosphorylated HP1γ (pHP1γ; Fig. 1 D and Fig. S2), indicative of senescence-associated heterochromatin foci (SAHF; Adams, 2007). At 12 mo, most of PIN cells in PTEN$^{(i)pe-/-}$ mice exhibited staining for senescence-associated β-galactosidase (SA-βGal), a well-accepted marker of cell senescence (Dimri et al., 1995; Collado and Serrano, 2006), and ∼20–50% of PIN cells were SA-βGal positive at 2 and 5 mo, respectively (Fig. 1 E). In contrast, at 1 mo, only ∼7% of PEC were pHP1γ-positive in PTEN$^{(i)pe-/-}$ mice, and almost no SA-βGal staining was observed. Transcript levels of several members of the senescence-associated secretory phenotype (SASP; e.g., *IL-1α*, *IL-1β*, *M-CSF*, and *TNFα*) (Pérez-Mancera et al., 2014) were increased by 4- to 15-fold at 2 and 5 mo in the prostate of PTEN$^{(i)pe-/-}$ mice, whereas their levels were similar in control and PTEN$^{(i)pe-/-}$ mice at 1 mo (Fig. 2). Thus, *PTEN* deficiency stimulates the proliferation of PECs within 1 mo to form PINs, which become progressively senescent within the following months.

PTEN deficiency in PECs induces replication stress

Because DDR is an inducer of OIS (Bartkova et al., 2006; Di Micco et al., 2006; Mallette et al., 2007), we investigated the levels of phosphohistone H2AX S139 (γH2AX), a faithful marker of DDR activation (Rogakou et al., 1998; Mah et al., 2010). Western blot analysis showed increased levels of γH2AX in DLP extracts of PTEN$^{(i)pe-/-}$ mice at 1 mo (Fig. S3 A), and immunohistological analyses revealed that most PECs in DLP of PTEN$^{(i)pe-/-}$ mice present a nuclear staining of γH2AX, whereas no staining was observed in the prostatic epithelium of age-matched control

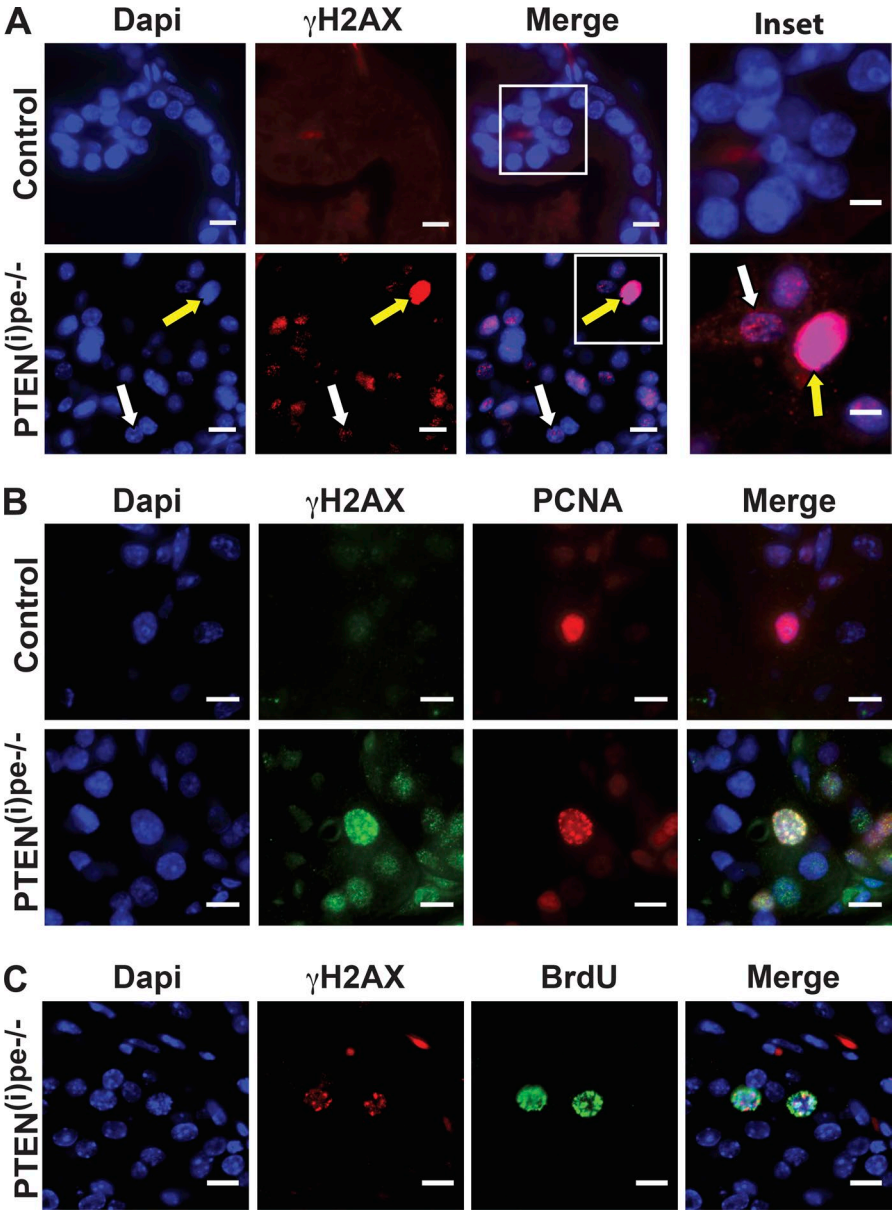

Figure 3. **Characterization of replication stress in *PTEN*-deficient PECs. (A)** Representative γH2AX immunofluorescence staining (red) of DLP sections of PTEN$^{(i)pe-/-}$ and control mice sacrificed 1 mo after gene ablation. Yellow arrow, example of γH2AX-high staining; white arrow, example of γH2AX-low staining. **(B)** Representative immunofluorescence staining of γH2AX (green) and PCNA (red) of a DLP section of a PTEN$^{(i)pe-/-}$ and of a control mouse sacrificed 1 mo after gene ablation. **(C)** Representative immunofluorescence staining of γH2AX (red) and BrdU (green) of a DLP section of a PTEN$^{(i)pe-/-}$ mouse sacrificed 1 mo after gene ablation. Blue, Dapi. Bars: main images, 10 µm; insets, 5 µm. Four PTEN$^{(i)pe-/-}$ mice and four control mice were analyzed.

mice (Fig. 3 A). Although most cells displayed numerous small nuclear foci, ∼5% of the cells exhibited a very intense γH2AX nuclear staining (γH2AX-high), and often, no individual γH2AX foci could be distinguished in these cells (Fig. 3 A). Importantly, γH2AX-high PECs stained positive for the proliferation marker PCNA (Fig. S3 B), and individual γH2AX foci colocalized with foci of PCNA (Fig. 3 B). In contrast, no γH2AX foci were observed in PCNA-positive PECs of age-matched control mice. Therefore, in γH2AX-high PECs, γH2AX foci are localized at the vicinity or at the site of DNA replication, which is characteristic of replication stress (Ward and Chen, 2001). In addition, labeling of DNA-replicating cells with BrdU revealed that all γH2AX-high PECs were BrdU-positive in PTEN$^{(i)pe-/-}$ mice (Fig. 3 C). Moreover, at 1 and 2 mo, PECs of PTEN$^{(i)pe-/-}$ mice displayed numerous nuclear foci of RPA32, a subunit of the single-stranded genomic DNA (ssDNA) complex replication protein A (RPA) that coats stretches of ssDNA in replication stress (Branzei and Foiani, 2005; Byun et al., 2005), although such foci were rarely observed in prostatic epithelial cells of age-matched control mice (Fig. 4 A and not depicted). RPA phosphorylation at various sites occurs at stalled replication forks, and DNA double strand breaks (DSB) produced from stalled DNA replication induce phosphorylation of RPA32 at S4 and S8 (Liaw et al., 2011; Sirbu et al., 2011). Interestingly, at 1 mo, many PEC nuclei of PTEN$^{(i)pe-/-}$ mice contained high levels of S4/S8 phosphorylated RPA32 (Fig. 4 B), indicating that DSB follow replication fork stalling. Numerous nuclear foci of ATR (Ataxia telangiectasia and Rad3-related) and 53BP1 (p53-binding protein 1) were also observed in PECs of PTEN$^{(i)pe-/-}$ mice, whereas none were observed in PECs of age-matched control mice (Fig. 4, C and D), further supporting activation of DDR signaling (Cortez et al., 2001; Lukas et al., 2011). Together these results show that replication stress-mediated DDR signaling is induced in proliferating *PTEN*-deficient PECs. In agreement with the DDR mediating senescence induction, discrete foci of γH2AX were present in most PIN cells of PTEN$^{(i)pe-/-}$ mice at 5 mo (Fig. S3 C), similar to long term γH2AX foci observed in OIS (Rodier et al., 2011).

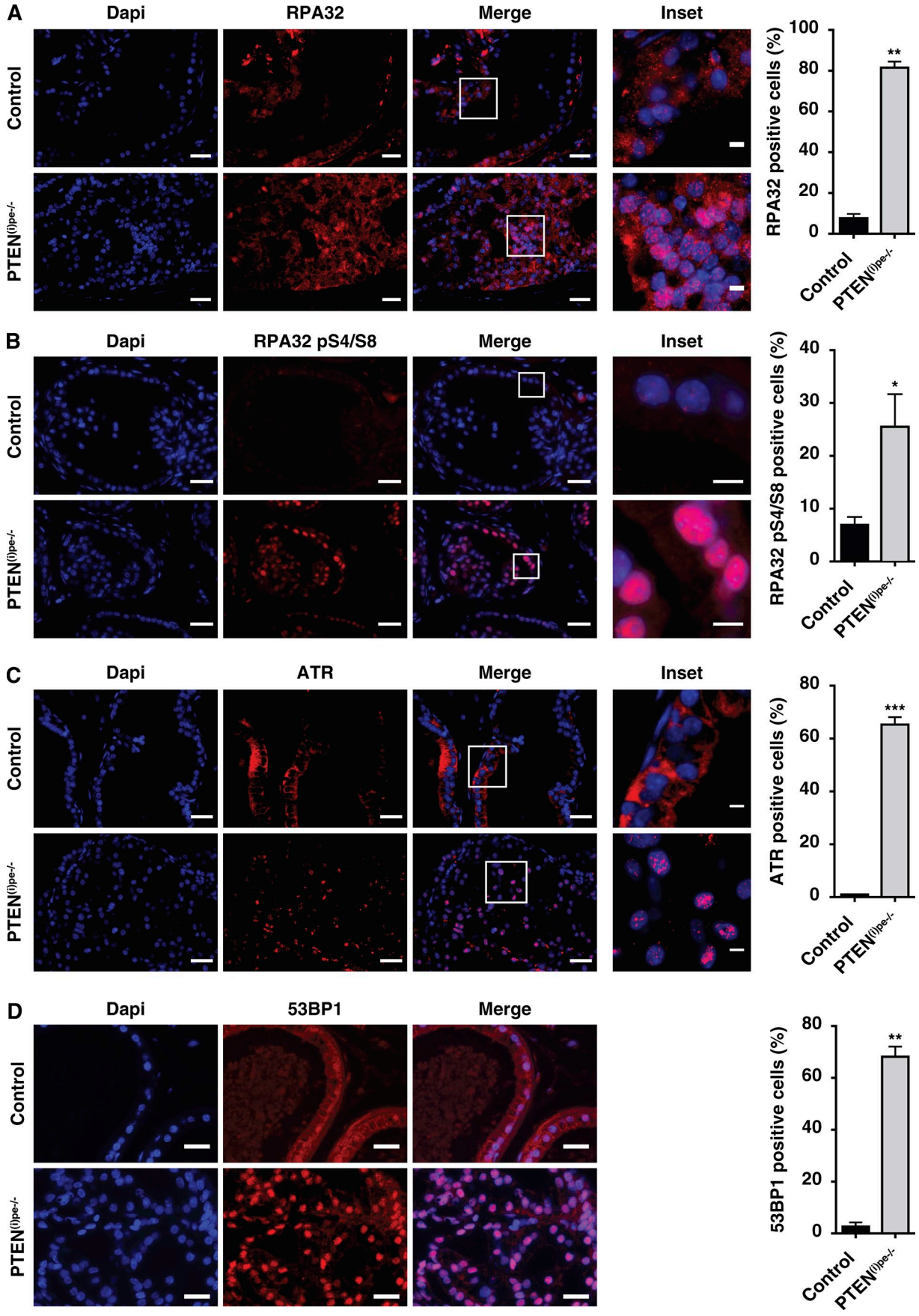

DDR stabilizes p53 in proliferating PECs of PTEN$^{(i)pe-/-}$ mice.
Because p53 can be stabilized by the DDR (Meek, 2009), we immunodetected p53. Nuclear accumulation of p53 was observed in >90% PECs of PTEN$^{(i)pe-/-}$ mice at 2 mo, whereas almost all PECs displayed nuclear p53 at 5 and 12 mo (Fig. 5 A and Fig. S4 A). No p53-positive nuclei were detected in prostate epithelium of control mice at any time point. Therefore, *PTEN* ablation induced nuclear accumulation of p53 in PECs within 2 mo and up to 12 mo. In contrast, at 1 mo, only ∼6% of PECs were p53-positive in PTEN$^{(i)pe-/-}$ mice (Fig. 5 A and Fig. S4 A), and most of them were Ki67- and BrdU-positive (Fig. 5 B and Fig. S4 B). This is in agreement with the slightly increased expression of the p53-target gene p21 at 1 mo (Fig. 1 C) and shows that activation of p53 signaling precedes senescence.

Activation of the DDR increases p53 stability and its transcriptional activity through phosphorylation of its serine 15 (Meek, 2009). p53 pS15 nuclear staining was observed in ∼5% PECs of PTEN$^{(i)pe-/-}$ mice at 1 mo, and these cells also stained for the proliferation marker Ki67 (Fig. 5 C). Therefore, p53 is stabilized in proliferating PECs of PTEN$^{(i)pe-/-}$ mice by a DDR-mediated pathway.

p53 stabilization is counteracted by the protein kinase B (AKT)–Mdm2 axis.
To investigate the role of p53 in the control of senescence induced by *PTEN* loss, we administered Tam to 8-wk-old PSA-CreER^{T2} mice bearing LoxP-flanked *PTEN* and *p53* alleles to generate PTEN/p53$^{(i)pe-/-}$ mice in which both *PTEN* and *p53* are ablated in PECs at adulthood.

As expected, no nuclear staining for p53 was observed in PECs of PTEN/p53$^{(i)pe-/-}$ mice (Fig. S4, C and D). At 1 and 2 mo, the prostate weights were similar in PTEN/p53$^{(i)pe-/-}$ and in PTEN$^{(i)pe-/-}$ mice (Fig. 6 A). The mitotic index of PECs was similar in PTEN/p53$^{(i)pe-/-}$ and PTEN$^{(i)pe-/-}$ mice at 1 mo, but was higher in PTEN/p53$^{(i)pe-/-}$ mice than in PTEN$^{(i)pe-/-}$ at 2, 5, and 6 mo (Fig. 6 B). At 5 and 6 mo, the prostate weight was threefold higher in PTEN/p53$^{(i)pe-/-}$ than in PTEN$^{(i)pe-/-}$ mice (Fig. 6 A). Whereas PIN lesions in DLP were similar in PTEN/p53$^{(i)pe-/-}$ and in PTEN$^{(i)pe-/-}$ mice at 1 and 2 mo, they were more severe in PTEN/p53$^{(i)pe-/-}$ mice than in PTEN$^{(i)pe-/-}$ mice at 5 and 6 mo with, in some cases, a loss of prostate epithelium architecture (compare Fig. 6 C and Fig. S1 C). Therefore, *p53* ablation does not affect early stimulation of *PTEN*-null PEC proliferation and PIN formation, but impairs their subsequent growth arrest.

Di Mitri et al. reported that GR1-positive myeloid cells infiltrate the prostate of PTEN$^{pe-/-}$ mice and secrete the cytokine IL-1RA, an antagonist of IL-1R, which opposes PICS in a paracrine fashion (Di Mitri et al., 2014). FACS analysis of dissociated prostates of PTEN$^{(i)pe-/-}$ mice revealed that GR-1–positive myeloid cells represent ∼2.5–3% of all prostatic cells at 2 and 5 mo after *PTEN* ablation, but <0.07% at 1 mo in both in PTEN$^{(i)pe-/-}$ and control mice (Fig. 7 A). Moreover, the transcript levels of the marker of the myeloid lineage *CD11b*, and of *Ly6g* and *Ly6c*, the two GR-1 variants, were increased in PTEN$^{(i)pe-/-}$ mice at 2 and 5 mo, but not at 1 mo (Fig. 7, B–D). In agreement with these results, the transcript levels of *IL-1rn*, coding for IL-1RA protein, were markedly increased at 2 and 5 mo in the prostate PTEN$^{(i)pe-/-}$ mice, whereas they were similar in control and PTEN$^{(i)pe-/-}$ mice at 1 mo (Fig. 7 E). Therefore, IL-1RA–producing GR-1–positive cells cannot account for the delay of PEC senescence entry induced by *PTEN* ablation.

In unstressed cells, p53 is maintained at low level by proteasomal degradation through mouse double-minute 2 (Mdm2)-mediated polyubiquitylation (Rodriguez et al., 2000). Stabilization of p53 involves the dissociation of p53 from Mdm2 through modifications of p53, including phosphorylation by DDR kinases ATR or ATM. Once stabilized, p53 translocates to the nucleus, whereas Mdm2 is submitted to proteasomal degradation. At 1 mo, high levels of Mdm2 were present in the nuclei of pAKT S473–positive PECs of PTEN$^{(i)pe-/-}$ mice (Fig. 8 A). Moreover, Mdm2-positive cells were p53-negative, and p53 was only detected in Mdm2-low cells (Fig. 8 B). To demonstrate that Mdm2 was involved in p53 degradation at early time, PTEN$^{(i)pe-/-}$ mice were treated with Nutlin-3, an inhibitor of Mdm2–p53 interaction (Vassilev et al., 2004) 1 mo after *PTEN* ablation. Our results show that Nutlin-3a treatment increases p53 protein levels in prostatic epithelial cells and enhances the transcript levels of p53 target gene *p21* (Fig. 8, C–E). Thus, low p53 levels at early time result from Mdm2-mediated p53 degradation.

Because AKT can phosphorylate Mdm2 at several serine residues (S166 and S186 in human, equivalent to S163 and S183, in mouse), inducing its nuclear translocation and accumulation (Feng et al., 2004; Wei et al., 2013), and increasing both its association and E3 ligase activity toward p53 (Ashcroft et al., 2002; Mayo et al., 2002; Ogawara et al., 2002), AKT might promote Mdm2-mediated p53 proteasomal degradation in PECs of PTEN$^{(i)pe-/-}$ mice. Importantly, most nuclei of PECs were Mdm2 pS163–positive at 1 mo, whereas Mdm2 pS163 was not immunodetected in normal prostate epithelium of PTEN$^{(i)pe-/-}$ mice and of control mice (Fig. 9 A and not depicted). The level of Mdm2 pS163 decreased, however, between 1 and 2 mo, while p53 increased and was detected in most cells at 5 mo, whereas Mdm2 pS163 was detected no more (Fig. 9 A and Fig. 5 A). Moreover, because Casein Kinase I (CKI) family members have been shown to phosphorylate N-terminal sites of p53 and to decrease p53 affinity to Mdm2, and because phosphorylation of Mdm2 by CKIδ leads to Mdm2 degradation and p53 expression (Knippschild et al., 2014), we determined their transcript levels in *PTEN*-deficient PINs at various time points. Interestingly, the transcript levels of *CKIα*, *-δ*, *-γ*, and *-ε* were induced 3 and 5 mo after gene invalidation, and at 5

Figure 4. **Immunodetection of DDR markers in *PTEN*-deficient PECs. (A)** Representative immunofluorescence staining of RPA32 (red) of DLP sections of PTEN$^{(i)pe-/-}$ or control mice sacrificed 2 mo after gene ablation. **(B)** Representative RPA32 pS4/S8 immunofluorescence staining (red) of DLP sections of PTEN$^{(i)pe-/-}$ and control mice sacrificed 1 mo after gene ablation. **(C)** Representative ATR immunofluorescence staining (red) of DLP sections of PTEN$^{(i)pe-/-}$ and control mice sacrificed 2 mo after gene ablation. **(D)** Representative immunofluorescence staining of 53BP1 (red) of DLP sections of PTEN$^{(i)pe-/-}$ or control mice sacrificed 2 mo after gene ablation. Blue, Dapi. Bars: main images, 20 µm; insets, 5 µm. Four PTEN$^{(i)pe-/-}$ mice and four control mice were analyzed. A quantification of immunolabeled epithelial cells is shown in each panel. *, P value < 0.05; **, P value < 0.01; ***, P value < 0.001.

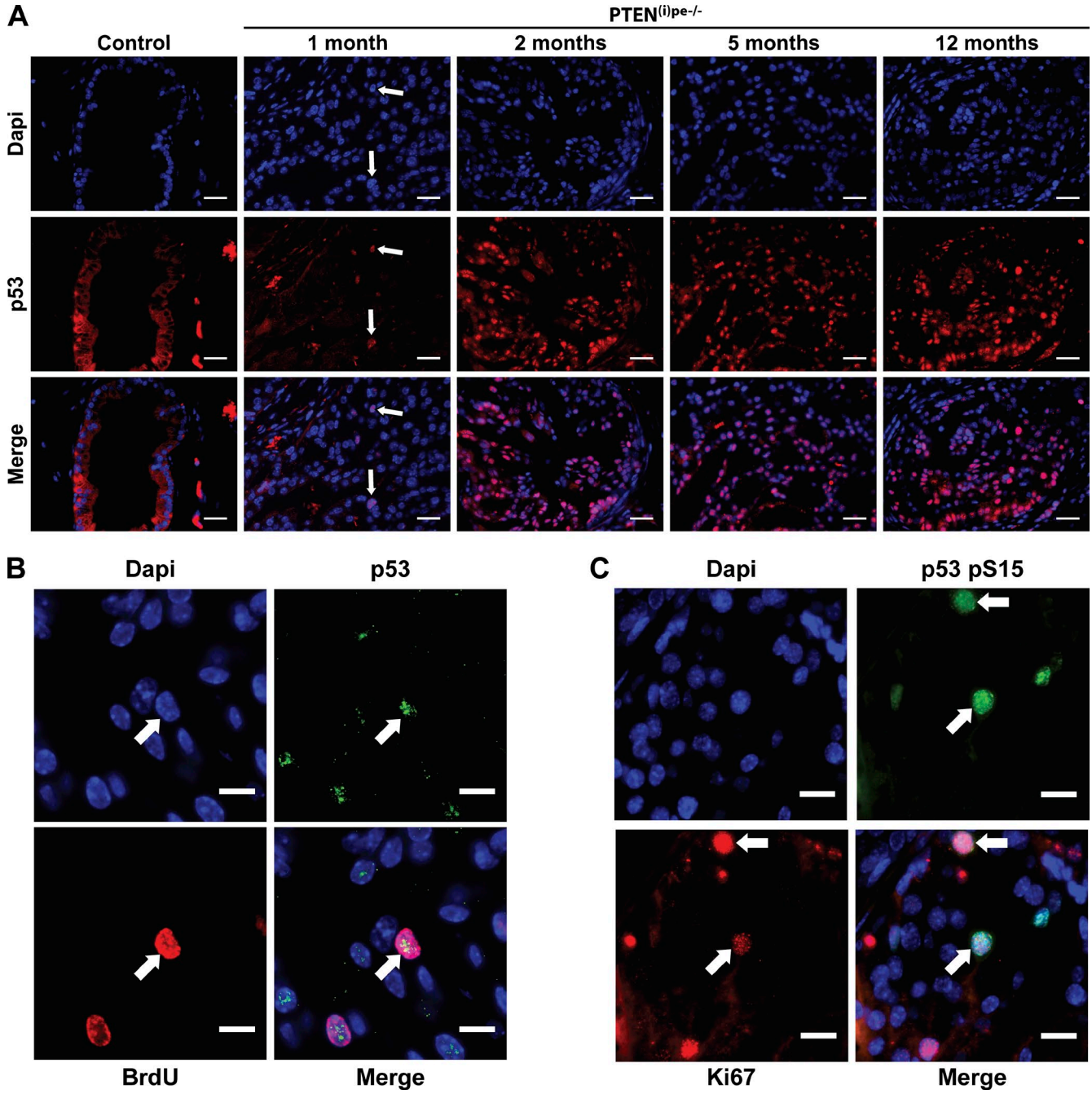

Figure 5. **Characterization of p53-positive *PTEN*-deficient PECs. (A)** Representative p53 immunofluorescence staining (red) of DLP sections of PTEN$^{(i)pe-/-}$ and control mice sacrificed at indicated time points after gene ablation. White arrow, example of a stained nucleus at 1 mo. **(B)** Representative BrdU (red) and p53 (green) immunofluorescence staining of DLP sections of PTEN$^{(i)pe-/-}$ and control mice sacrificed 1 mo after gene ablation. White arrow, example of a double-stained nucleus. **(C)** Representative p53 pS15 (green) and Ki67 (red) immunofluorescence staining of DLP sections of PTEN$^{(i)pe-/-}$ and control mice sacrificed 1 mo after gene ablation. White arrow, example of a double-stained nucleus. Blue, Dapi. Bars: 25 µm (A); 10 µm (B and C). Four PTEN$^{(i)pe-/-}$ mice and four control mice were analyzed.

mo, the transcript levels of *CKIε* correlated with *p21* levels (Fig. 9, B and C; and Fig. S5).

Thus, as DNA damage has been shown to induce the interaction between Mdm2 and CKI (Inuzuka et al., 2010), it is likely that 3 mo after *PTEN* ablation, CKI-mediated Mdm2 degradation, and/or decreased binding of Mdm2 to p53 overcomes early Mdm2 activation and contributes to p53 stabilization.

Discussion

We show here that *PTEN* ablation in PECs of adult mice induces PINs formation, the progression of which is antagonized by a cell senescence barrier, in agreement with previous studies (Chen et al., 2005; Di Mitri et al., 2014). Because PTEN knockdown in cultured cells was shown to induce a rapid senescence state in the absence of proliferation and DDR, in contrast to OIS

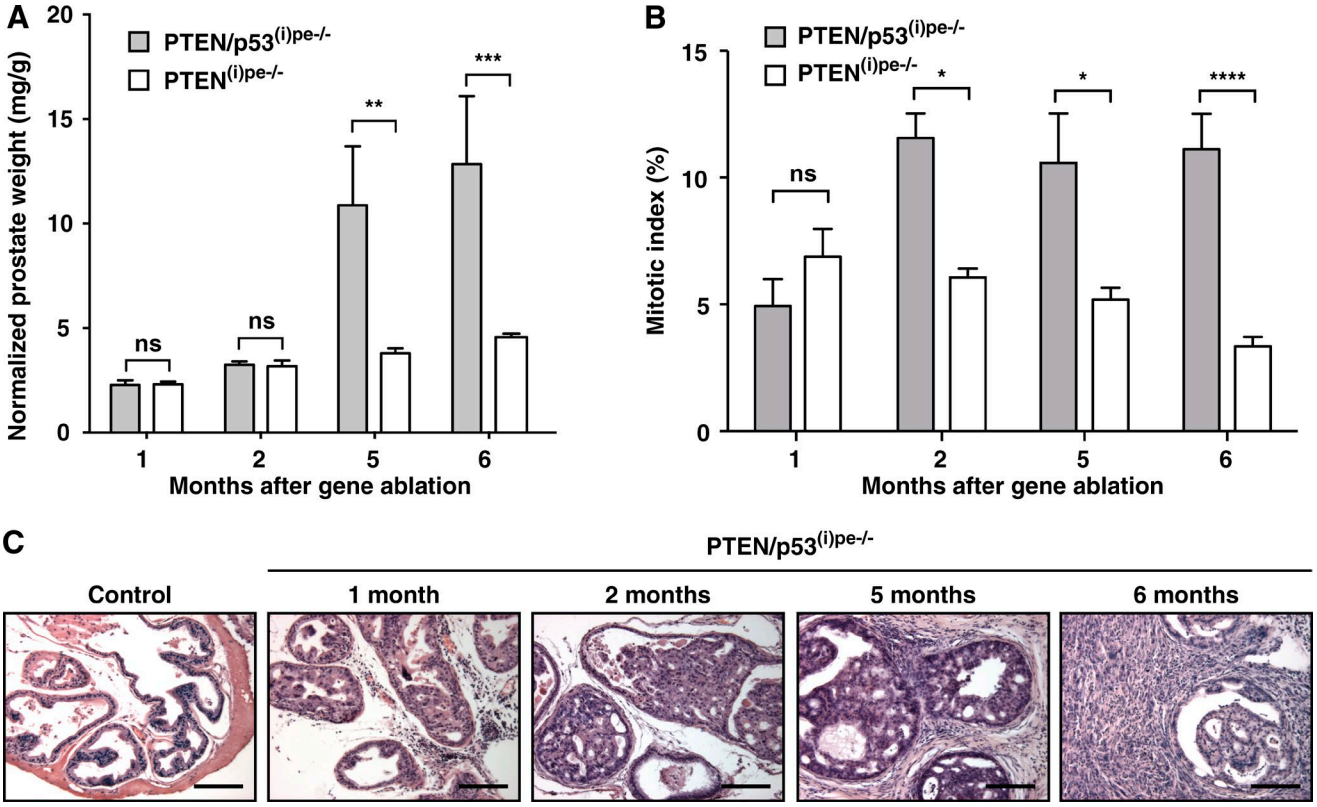

Figure 6. **Prostate tumor evolution in PTEN/p53$^{(i)pe-/-}$ mice. (A)** Evolution of normalized prostate weight (prostate weight over body weight) in PTEN$^{(i)pe-/-}$ and PTEN/p53$^{(i)pe-/-}$ mice over 6 mo after gene ablation. Values are mean from of four to eight mice ± SEM. **(B)** Proliferation index (percentage of Ki67-positive cells) of DLP epithelial cells in PTEN$^{(i)pe-/-}$ and PTEN/p53$^{(i)pe-/-}$ mice over 6 mo after gene ablation. Values are mean from of four to eight mice ± SEM. **(C)** Representative views of DLP sections of PTEN/p53$^{(i)pe-/-}$ and control mice sacrificed at 1, 2, and 5 mo after gene ablation and of DLP sections of PTEN/p53$^{(i)pe-/-}$ mice with large tumors, sacrificed 6 mo after gene ablation. Sections were stained with H&E. Bars, 125 µm. Four to eight PTEN/p53$^{(i)pe-/-}$ mice per time point and eight control mice were analyzed. ns, not significant, P value ≥ 0.05; *, P value < 0.05; **, P value < 0.01; ***, P value < 0.001; ****, P value < 0.0001.

(Alimonti et al., 2010; Astle et al., 2012), it was proposed that PICS is a new type of senescence. Moreover, it was shown that PICS is antagonized by IL-1RA secreted by infiltrated GR1-positive myeloid cells, allowing proliferation of a subset of *PTEN*-deficient PECs and, thereby, PIN formation (Alimonti et al., 2010; Di Mitri et al., 2014).

We demonstrate here that GR1-positive cells and IL-1RN are not present in the prostate 1 mo after *PTEN* ablation in PTEN$^{(i)pe-/-}$ mice and, thus, cannot contribute to the high proliferation rate and the absence of senescence markers at this stage. Therefore, we conclude that the first temporal consequence of *PTEN* ablation in mouse PECs is to increase their rate of proliferation, allowing PIN formation in most prostate ducts within 1 mo. Signs of senescence are observed only later, after several weeks of active proliferation.

Unlike previous studies (Alimonti et al., 2010; Astle et al., 2012), *PTEN* ablation in PECs induced γH2AX nuclear foci, clearly reflecting activation of the DDR. Our results are in agreement with a previous study showing that PTEN knock-down in human-immortalized fibroblasts induces cell senescence with accumulation of γH2AX foci (Kim et al., 2007). Importantly, proliferating PECs in PTEN$^{(i)pe-/-}$ mice displayed a very strong γH2AX staining, with numerous intense foci, and presented characteristics of replication stress, including accumulation of foci of RPA32 and RPA32 pS4/S8, as well as ATR, the DDR kinase activated by replication stress and a major effector of replication stress–mediated DDR (Mazouzi et al., 2014).

ATR can phosphorylate p53 S15 directly or via activation of CHK1 (Mazouzi et al., 2014), and our results show that actively proliferating cells exhibit a nuclear staining for p53 pS15 and that p53 mainly accumulates in Ki67-positive and BrdU-positive PECs. Therefore, p53 is stabilized by replication stress–mediated DDR activation in *PTEN*-deficient PECs, and replication stress–mediated p53 activation contributes to trigger senescence, as in OIS (Bartkova et al., 2006; Bartek et al., 2007).

In addition, we show that Mdm2 accumulates in the nuclei of AKT pS473–positive PECs at 1 mo and that nuclear Mdm2 is phosphorylated at S163. It is well documented that Mdm2 can be phosphorylated at S163 by AKT, resulting in its translocation in the nucleus, while it increases its E3-ligase activity toward p53 and thus down-regulates p53 (Mayo and Donner, 2001; Mayo et al., 2002; Ogawara et al., 2002; Feng et al., 2004; Fenouille et al., 2011). It has been shown that *PTEN* ablation in mouse cells and tissue results in a dramatic decrease of p53 expression (Freeman et al., 2003), and pharmacological inhibition of PI3K prevents p53 activation by DNA damage (Bar et al., 2005). Moreover, activation of AKT by Her2 in breast cancer cells increases Mdm2-mediated p53 degradation via AKT-mediated Mdm2 phosphorylation on S163 (Zhou et al., 2001). Importantly, we show that early p53 degradation in *PTEN*-deficient PECs is mediated by Mdm2 and

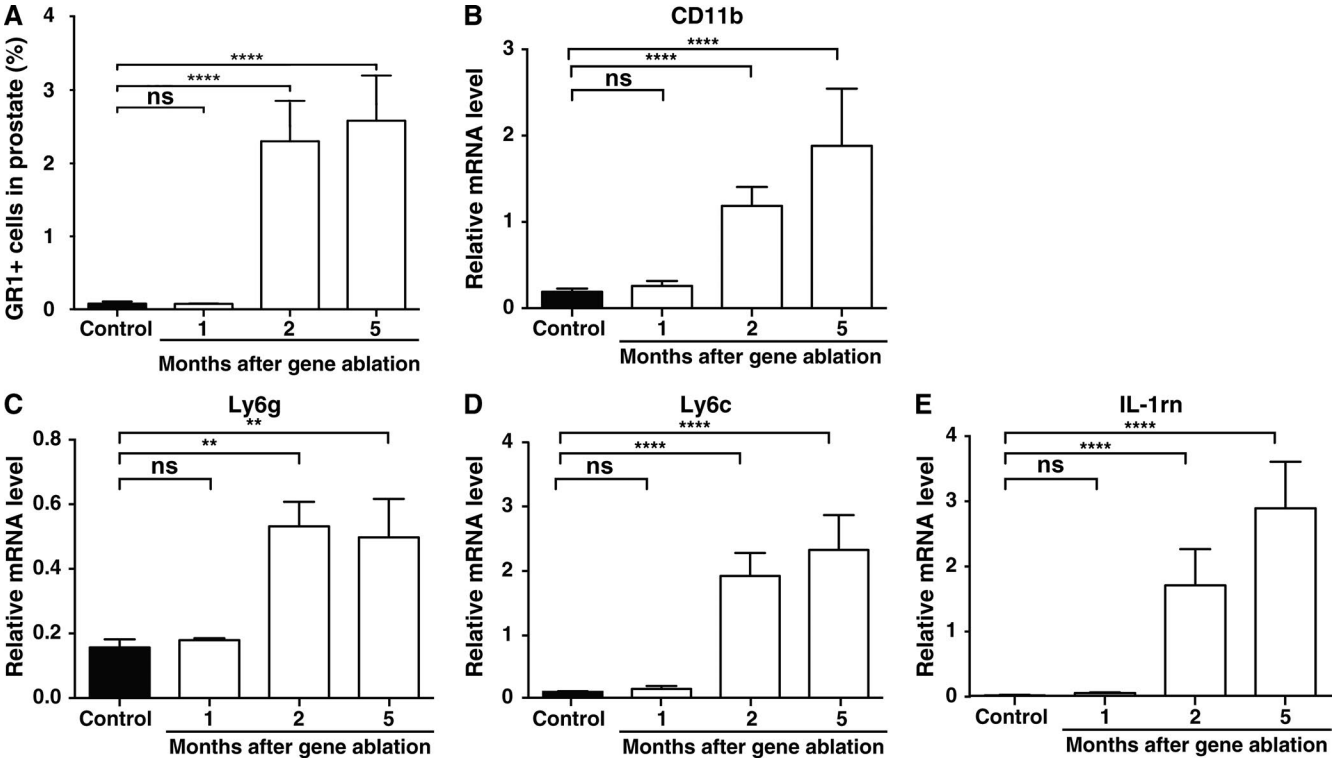

Figure 7. **Characterization of GR1-positive myeloid cells and *IL1rn* expression during PIN evolution in PTEN$^{(i)pe-/-}$ mice. (A)** FACS quantification of GR1-positive myeloid (CD11b-positive) cells in the prostate of PTEN$^{(i)pe-/-}$ and control mice (percentage of the total cells in dissociated prostates) sacrificed at the indicated time points after gene ablation. **(B–E)** Values are mean of three to six mice ± SEM. Relative transcript levels of *CD11b* (B), *Ly6g* (C), *Ly6c* (D) and *IL-1rn* (E) in the prostate of PTEN$^{(i)pe-/-}$ and control mice sacrificed at indicated time points after gene ablation. Values are mean of four to ten mice ± SEM. ns, not significant, P value ≥ 0.05; **, P value < 0.01; ****, P value < 0.0001.

provide evidence that CKI contributes to p53 stabilization at later time. We thus propose that *PTEN* loss has two simultaneous and opposed consequences. Besides initiating a senescence program through replication stress mediated activation of the DDR and p53 stabilization, AKT activation induced by *PTEN* ablation contributes to delay senescence via enhanced Mdm2-mediated p53 degradation.

An important characteristic of our mouse model is the possibility to strictly control the time of floxed genes ablation by induction of the CreER^{T2} recombinase activity. In other models, *PTEN* ablation occurs in the undifferentiated prostate of young mice (Chen et al., 2005; Alimonti et al., 2010), because of the early activity of the Pb-4 promoter (in the prostate bud of the newborn) that drives the expression of a constitutively active Cre recombinase (Wu et al., 2001). As we induced Cre-mediated recombination selectively in luminal prostatic epithelial cells after puberty, *PTEN* was ablated in a fully developed prostate and well-differentiated PECs. It was shown that PIN development is accelerated when *PTEN* is ablated before puberty (Luchman et al., 2008). Thus, the lower proliferation rate of PECs in our model, which reaches a maximum of ∼10%, although it reaches ∼40% in previously studied models (Chen et al., 2005; Alimonti et al., 2010), might contribute to the slow establishment of cell senescence, as replication stress might be less intense.

Our results diverge from several published studies on PICS. The discrepancy between our observations made in vivo in epithelial cells and in vitro results obtained in nonepithelial cells (Alimonti et al., 2010; Astle et al., 2012) might result from the obvious growth conditions differences. Indeed, in vitro cell culture conditions induce cellular stress, because partial O_2 pressure is much higher in culture medium than in tissues, and because high levels of growth factors push the cells to actively proliferate (Serrano and Blasco, 2001). Thus, cells in culture might induce pathways to cope with such stress conditions. In any event, our data highlight that in vitro data on senescence should not be extrapolated to in vivo situations.

As we demonstrate here that *PTEN* loss–induced cell senescence in prostate epithelial cells is mediated at least in part by replication stress after a phase of enhanced proliferation in vivo, this type of senescence resembles other types of senescence, in particular OIS, in contrast to previous conclusions drawn from others (Alimonti et al., 2010). Thus, approaches for cancer prevention and therapy based on PICS induction are at risk, because replication stress induced by *PTEN* loss might result in an accumulation of mutations, including of *p53*, before p53 is stabilized and senescence initiated, and/or in senescent cells, leading to senescence escape and formation of adenocarcinoma. Supporting this idea, *p53* mutations cooccur with *PTEN* mutations in a high proportion of advanced prostate tumors (Chen et al., 2005; Lotan et al., 2011; Markert et al., 2011).

In contrast, selective inhibitors of AKT or of Mdm2-p53 interaction might enforce senescence and prevent or delay prostate cancer progression. However, the safest approach remains probably the elimination of senescent cells.

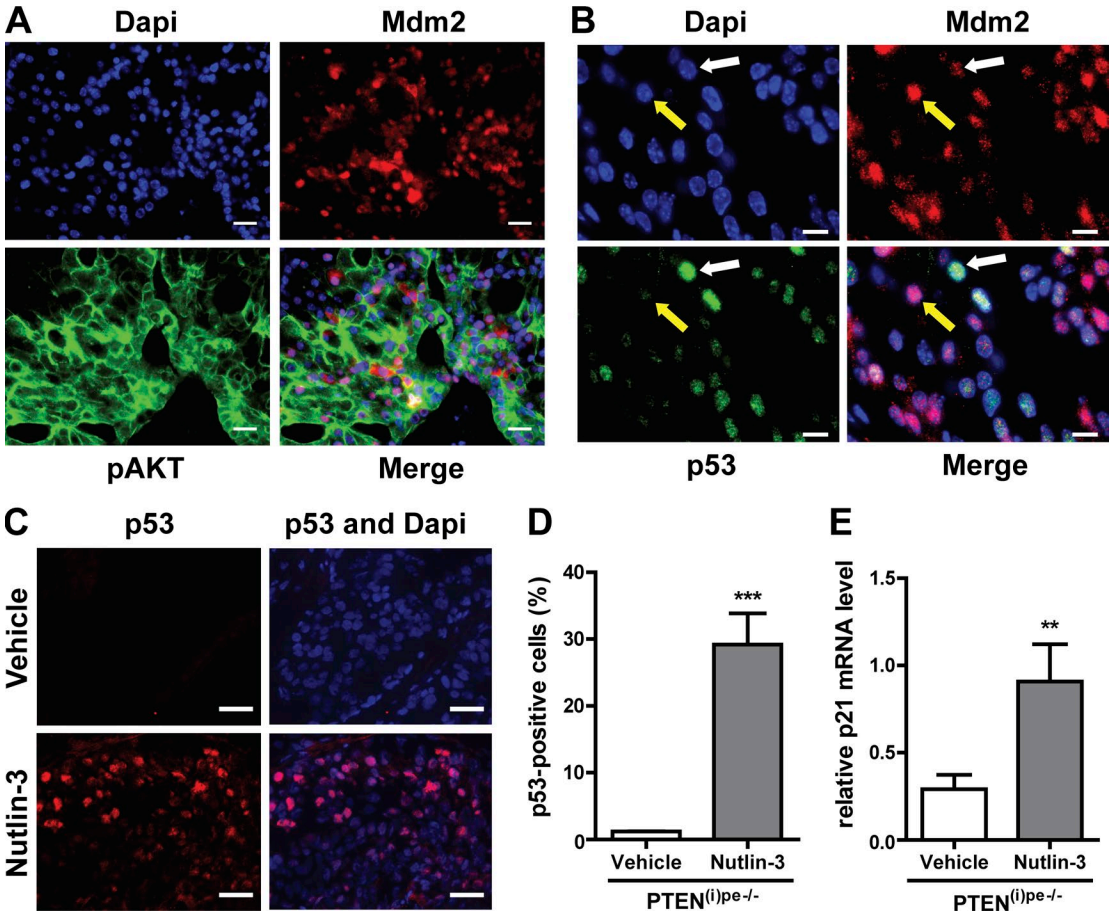

Figure 8. **Characterization of Mdm2 expression in the prostate of PTEN$^{(i)pe-/-}$ mice. (A)** Representative pAKT S473 (green) and Mdm2 (red) immunofluorescence staining of DLP sections of a PTEN$^{(i)pe-/-}$ mouse sacrificed 1 mo after gene ablation. Blue, Dapi. Four mice were analyzed. **(B)** Representative p53 (green) and Mdm2 immunofluorescence staining (red) of DLP sections of a PTEN$^{(i)pe-/-}$ mouse sacrificed 1 mo after gene ablation. Four mice were analyzed. **(C)** Representative p53 immunofluorescence staining (red) of DLP sections of PTEN$^{(i)pe-/-}$ mice treated with vehicle- and Nutlin-3 1 mo after gene ablation (n = 3 for each condition). Blue, Dapi. Bars: 20 µm (A and C); 10 µm (B). Data are representative of two experiments; n = 3 vehicle and n = 3 Nutlin-treated PTEN$^{(i)pe-/-}$ mice. **(D)** Quantification of p53 positive epithelial cells in PINs of PTEN$^{(i)pe-/-}$ mice treated 1 mo after gene ablation with vehicle and Nutlin-3. Data are cumulative of two experiments; n = 3 for each group. Unpaired-t test. ***, P value < 0.001. **(E)** Relative transcript levels of *p21* in the DLP and AP of vehicle- and Nutlin-3 treated PTEN$^{(i)pe-/-}$ mice. n = 7 vehicle and n = 8 Nutlin-3 treated PTEN$^{(i)pe-/-}$ mice. Unpaired-t test. **, P value <0.01.

Materials and methods

Mouse care

Mice were maintained in a temperature- and humidity-controlled animal facility with a 12 h light/dark cycle. Breeding and maintenance of mice were performed in the accredited IGBMC/ICS animal house (C67-2018-37), in compliance with French and EU regulations on the use of laboratory animals for research, under the supervision of D. Metzger who holds animal experimentation authorizations from the French Ministry of Agriculture and Fisheries (Nos. 67-209 and A 67-227). All animal experiments were approved by the Ethical committee Com'Eth (Comité d'Ethique pour l'Expérimentation Animale, Strasbourg, France). Animals were euthanized with carbon dioxide and cervical dislocation, and tissues were immediately collected, weighed and frozen in liquid nitrogen, or processed for biochemical and histological analysis.

Generation of mouse cohorts

PTEN$^{(i)pe-/-}$ mice were generated as described (Ratnacaram et al., 2008). In brief, mice carrying one copy of the PSA-Cre-ER^{T2} transgene, expressing the Tam-inducible Cre-ER^{T2} recombinase in prostate epithelium under the control of the human PSA promoter, were crossed with mice carrying LoxP-flanked (floxed) alleles of *PTEN* (L2 allele; a gift from T. Mak, Campbell Family Institute for Breast Cancer Research, Toronto, Canada, and A Suzuki, Akita University School of Medicine, Akita, Japan) to generate PSA-Cre-ER$^{T2(tg/0)}$/PTEN$^{L2/L2}$ (tg, transgenic) and PSA-Cre-ER$^{T2(0/0)}$/PTEN$^{L2/L2}$ mice. PTEN/p53$^{(i)pe-/-}$ mice were generated by intercrossing PSA-Cre-ER$^{T2(tg/0)}$/PTEN$^{L2/L2}$ mice with p53$^{L2/L2}$ mice carrying floxed alleles of *p53* (a gift of A. Berns, The Netherlands Cancer Institute, Amsterdam, Netherlands; Jonkers et al., 2001) to generate PSA-Cre-ER$^{T2(tg/0)}$/PTEN$^{L2/L2}$/p53$^{L2/L2}$ and PSA-Cre-ER$^{T2(0/0)}$/PTEN$^{L2/L2}$/p53$^{L2/L2}$ mice. Gene ablation was induced by intraperitoneal injection of Tam performed daily for 5 d (1 mg/mouse) to 8- to 10-wk-old mice, as described (Fig. S1 A; Metzger et al., 2005), to generate mutant PTEN$^{(i)pe-/-}$ and PTEN/p53$^{(i)pe-/-}$ mice. Respective control mice (PTEN$^{pe+/+}$ and PTEN/p53$^{pe+/+}$) did not bear the PSA-Cre-ER^{T2} transgene (pe, prostate epithelium; (i), induced).

PSA-Cre-ER^{T2}, PTEN$^{L2/L2}$, and p53$^{L2/L2}$ mice were backcrossed on C57BL/6 mice for more than eight generations before

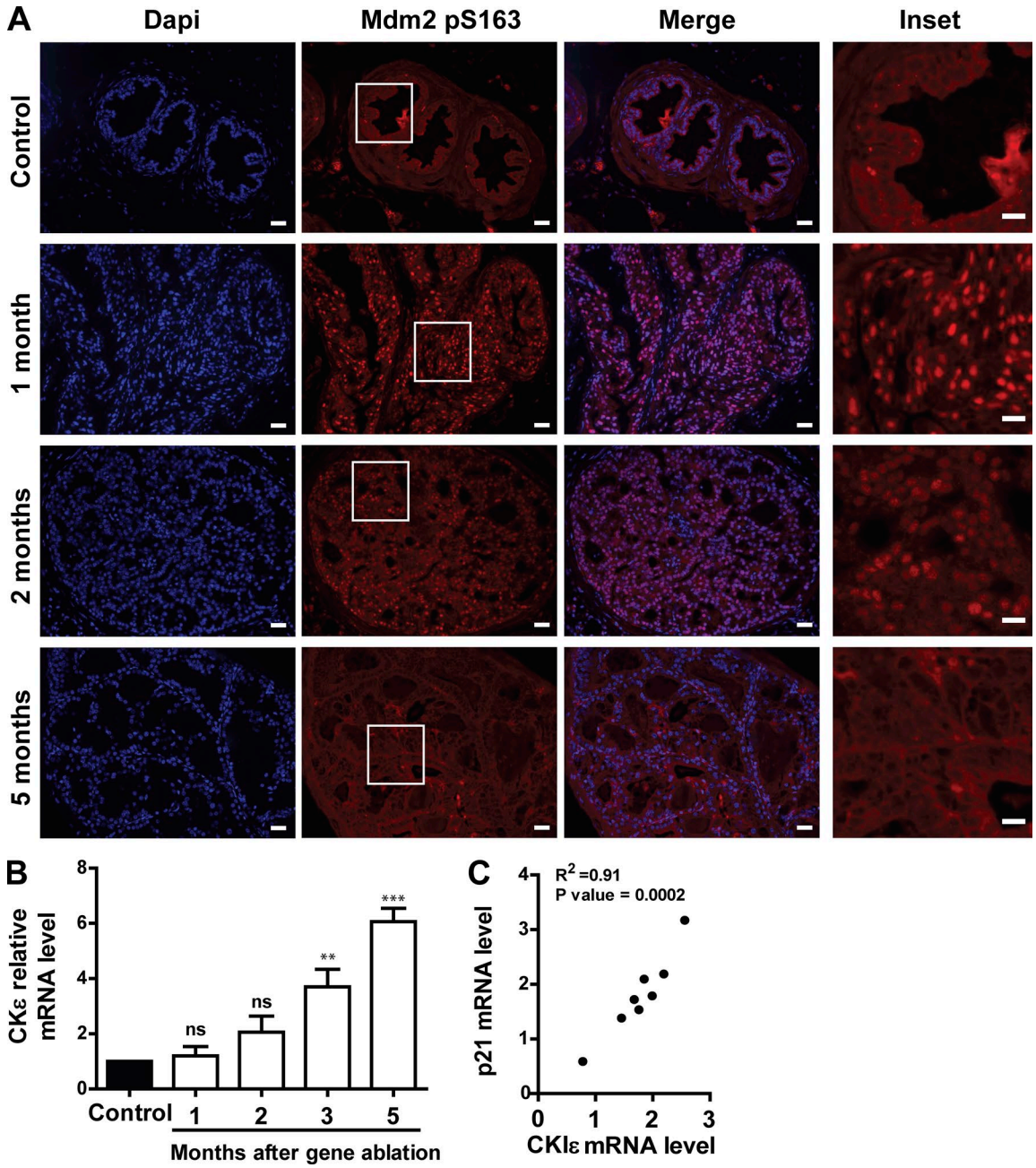

Figure 9. **Immunodetection of Mdm2 pS163 and quantification of *CKIε* and *p21* transcript levels in DLP of PTEN$^{(i)pe-/-}$ mice. (A)** Representative Mdm2 pS163 (red) immunofluorescence staining of DLP sections of control and PTEN$^{(i)pe-/-}$ mice sacrificed at the indicated time after gene ablation. Blue, Dapi. Bars: main images, 40 µm; insets, 10 µm. Data are representative of three experiments with $n = 3$ mice per time point and two prostate sections per mouse. **(B)** Transcript levels of *CKIε* in the DLP and AP of PTEN$^{(i)pe-/-}$ and control mice at the indicated time points. $n = 3$ for control mice at 5 mo and $n = 4$, $n = 4$, $n = 4$, $n = 3$, and $n = 8$ for PTEN$^{(i)pe-/-}$ mice at 1, 2, 3, and 5 mo after gene ablation, respectively. Bars represent the mean ± SEM. One way ANOVA. ns; not significant; **, P < 0.01; ***, P < 0.001. **(C)** Correlation between *p21* and *CKI1ε* transcript levels in the prostate of PTEN$^{(i)pe-/-}$ mice 5 mo after *PTEN* ablation.

intercrossing. Mice were genotyped by PCR performed on genomic DNA isolated from ear biopsies, using the DirectPCR extraction kit (102-T; Viagen) and primers as described (Jonkers et al., 2001; Ratnacaram et al., 2008).

Treatment of mice

Control and PTEN$^{(i)pe-/-}$ mice were administered i.p. with 5-bromo-2'-deoxyuridine (BrdU, Sigma-Aldrich) at 50 mg/kg in 100 µl of sterile saline solution (0.9% NaCl), 3 h before sacrifice. 1 mo after gene ablation, PTEN$^{pe-/-}$ mice were treated (i.p.) with Nutlin-3 (daily 100 mg/kg; AdooQ Biosciences) or vehicle for 2 d and sacrificed 4 h after the last administration.

Histological analysis

Prostate tissue samples were immediately fixed in ice-cold 4% formaldehyde supplemented with 1 tablet/10 ml of PhoSTOP (04 906 837 001; Roche). Prostate samples were embedded in paraffin, and 5-µm serial sections were cut. For histopathological

analyses, paraffin sections were stained with H&E. For immunofluorescence staining, sections were processed as previously described (Ratnacaram et al., 2008), except that sections were incubated over night with primary antibodies diluted 1:200, unless indicated. Primary antibody used for immunofluorescence were directed against AKT pS473 (4060; Cell Signaling Technology), γH2AX (05-636; EMD Millipore; 1:600), p53 (CM5; Vector Labs), p53 pS15 (12571; Cell Signaling Technology), pHP1γ (2600; Cell Signaling Technology), RPA32 (GTX113004; Tebu-Bio), RPA32 pS4/S8 (A300-245A; Bethyl Laboratories), ATR (2790; Cell Signaling Technology), Ki67 (M7248; Dako), BrdU (600-401-C29; Rockland), ATM pS1966 (200-301-400; Rockland), Mdm2 (sc-965; Santa Cruz Biotechnology), Mdm2 pS166 (human)/pS163 (mouse; 3521; Cell Signaling Technology), PCNA (ab2426; AbCam), 53BP1 (NB100-305; Novus Biologicals). Secondary antibodies (CY3 AffiniPure goat anti–rabbit IgG [H+L], CY3 AffiniPure goat anti–mouse IgG [H+L], CY5 AffiniPure goat anti–mouse IgG [H+L], and CY5 AffiniPure donkey anti–rabbit IgG [H+L]) were from Jackson Immunoresearch.

SA-βGal staining

10-µm frozen prostate sections were cut, fixed in 2% formaldehyde and 0.2% glutaraldehyde, stained in 100 mM $K_3Fe(CN)_6$, 100 mM $K_4Fe(CN)_6$, 2 mM $MgCl_2$, 150 mM NaCl, citric acid phosphate buffer (0.2 M Na_2HPO_4 and 0.1 M Citric acid), and 1 mg/ml X-gal (Roche) for 6 h and counterstained in hematoxylin (Dimri et al., 1995).

TUNEL assays

10-µm paraffin-embedded prostate sections were cut and stained with TUNEL kit (11684817910; In Situ Cell Death Detection kit; Roche) following manufacturer's instructions.

Microscope image acquisition

Microscopic analyses were performed at 21°C using a Leica Microsystems DM4000B with the following objectives: 10×, N Plan, dry, numerical aperture (NA): 0.25; 20×, HC Plan Apo dry, NA: 0.7; 40×, N Plan, dry, NA: 0.65; 63×, HCX Plan Apo, oil immersion, NA: 1.32–0.6; and 100, HCX PL Fluotar, oil immersion, NA: 1.30–0.6. Images were acquired with a 12-bit Photometrics Cool Snap FX camera by the Micro-Manager software. Pictures were edited with the Fiji software (Schindelin et al., 2012). The Cell Counter Fiji plugin was used for quantification of pathological features and histological markers.

RNA extraction and analysis

RNA was isolated from DLP and anterior prostate samples, and quantitative PCR of retrotranscribed RNAs were performed as described (Gali Ramamoorthy et al., 2015). Primer sequences were as follows: p16 forward: 5′-GAACTCTTTCGGTCGTACCC-3′, reverse: 5′-CAGTTCGAATCTGCACCGTA-3′; $p19^{ARF}$ forward: 5′-GCTCTGGCTTTCGTGAACAT-3′, reverse: 5′-GTGAACGTTGCC CATCATC-3′; p21 forward: 5′-TCTTCTGCTGTGGGTCAGGAG-3′, reverse: 5′-GAGGGCTAAGGCCGAAGATG-3′; IL-1α forward: 5′-AGACGGCTGAGTTTCAGTGAG-3′, reverse: 5′-TAAGGTGCT GATCTGGGTTG-3′; IL-1β forward: 5′-ACGACAAAATACCTG TGGCC-3′, reverse: 5′-TGGGTATTGCTTGGGATCCA-3′; M-CSF forward: 5′-GACCCAGGATGAGGACAGAC-3′, reverse: 5′-TTCCCA TATGTCTCCTTCCA-3′; TNFα forward: 5′-CACTTGGTGGTTTGC TACGA-3′, reverse: 5′-CCCCAAAGGGATGAGAAGTT-3′; IL-1rn forward: 5′-TGAGCTGGTTGTTTCTCAGG-3′, reverse: 5′-GAA AAGACCCTGCAAGATGC-3′; Ly6c forward: 5′-ATAGCACTCGTA GCACTGCA-3′, reverse: 5′-ACCTTGTCTGAGAGGAACCC-3′; Ly6g forward: 5′-TGTGCTCATCCTTCTTGTGG-3′, reverse: 5′-AGGGGC AGGTAGTTGTGTTG-3′; CD11b forward: 5′-CAAAGAACAACA CACGCAGG-3′, reverse: 5′-GGCTCCCCAACCAGTGTATA-3′; CKIε forward: 5′-TGAAGCATGGAGTTGCGTGT-3′, reverse: 5′-TGTTGG CACCCAGGTAGATG-3′; CKIα1 forward: 5′-TCCGCATCCTTTTCA GGACC-3′, reverse: 5′-AGAAACCTGTGGGGGTTTGG-3′; CKIδ forward: 5′-TACCTCACACACGGCCAACA-3′, reverse: 5′-GCAGCC GCATACTCACTTTC-3′; CKIγ1 forward: 5′-GGGTGGTTGAGAGAA GCAGT-3′, reverse: 5′-CCTGTCCTCCTAAATCAGCGG 3′; CKIγ2 forward: 5′-GCTATCAAGCTGGAGCCCAT-3′; reverse: 5′-TAGTAG ACCTGAGGGACGCC 3′; CKIγ3 forward: 5′-TGGCAAGGCTTAAAG GCTGA-3′; reverse: 5′-TGGGAAGTTCTCACACAACACT-3′; 18S forward: 5′- TCGTCTTCGAAACTCCGACT-3′, reverse: 5′-CGCGGT TCTATTTTGTTGGT-3′.

Preparation and analysis of prostate tissue protein extracts

Prostates were crushed in ice-cold modified radioimmunoprecipitation assay buffer (50 mM Tris, pH 7.5, 1% Nonidet P40, 0.5% sodium deoxycholate, 0.1% SDS, 150 mM NaCl, 5 mM EDTA, 5% glycerol, supplemented with protease inhibitor cocktail [05892970001; Sigma-Aldrich], PhoSTOP [PHOSS-RO; Sigma-Aldrich] and 1,4-dithiothreitol 10 mM) with a potter. Protein extracts (25 µg) were electrophoresed on 8–15% SDS-polyacrylamide gels and electroblotted to Hybond nitrocellulose membranes (Amersham Biosciences). Proteins were detected using primary antibodies directed against γH2AX (05-636; EMD Millipore; 1:1,000), AKT (4691; Cell Signaling Technology; 1:1,000), AKT pS473 (4060; Cell Signaling Technology; 1:1,000), and tubulin (TUB-2A2; IGBMC; 1:10,000). Membranes were probed with secondary HRP-conjugated secondary antibodies (Amersham Biosciences; 1:10,000), which were revealed using an enhanced chemiluminescence detection system (Pierce).

FACS analysis

Fresh prostates were chopped with a scalpel blade immediately after dissection, and dissociated for 4 h in 1 ml/50 mg of prostate tissue of dissociation buffer (RPMI-1640 cell culture medium [Thermo Fisher Scientific] supplemented with 10% heat-inactivated FBS, Hepes, pH 7.2, 10 mM, 200 µg/ml hyaluronidase [H3506; Sigma-Aldrich], 2.5 mg/ml collagenase [C0130; Sigma-Aldrich], and 25 mM $CaCl_2$) at 37°C with gentle shaking. After centrifugation (400 *g*; 5 min), pellets were washed twice with 10 ml of PBS and resuspended in 2 ml of prewarmed 0.05% trypsin (Thermo Fisher Scientific) supplemented with 5 mM EDTA. After a 5 min incubation at 37°C with gentle shaking, trypsin was inactivated by addition of RPMI-1640 supplemented with 10% heat-inactivated FBS, Hepes, pH 7.2, 10 mM, and 300 µg/ml DNase I (DN25; Sigma-Aldrich). Remaining cell clumps were physically dissociated by 10 passages through an 18-G needle and 10 passages through in a 20-G needle. After filtration on a 40-µm cell strainer, cell suspensions were centrifuged at 400 *g* for 5 min, washed twice in ice-cold PBS, and resuspended in

FACS buffer (PBS supplemented with 5 mM EDTA and 1% heat-inactivated FBS).

Cells were incubated with anti-CD16/32 antibodies (BD PharMingen; 1:50) for 15 min on ice to block nonspecific binding sites to Fc receptors, stained with antibodies directed against Epcam (PE-Cy7; Biolegend), CD45 (PerCP-Cy5.5; eBiosciences), CD11b (BV421; BD biosciences), and GR1 RB6-8C5 (FITC; eBiosciences; 1:50 each) for 15 min on ice, and analyzed on a BD LSR II Flow Cytometer (IGBMC; cytometry service) with FlowJo software. The presence of GR1-positive cells was determined by gating $CD11b^{high}GR1^{high}$ cells in $Epcam^{low}CD45^{high}$ cells. The proportion of $CD11b^{high}GR1^{high}$ cells was determined as the number of $CD11b^{high}GR1^{high}$ relative to the total number of single cells of dissociated prostate cells that were analyzed.

Statistical analysis

Statistical analysis was performed with the one-way ANOVA test with Prism (GraphPad).

Online supplemental material

Fig. S1 shows the generation and characterization of $PTEN^{(i)pe-/-}$ mice. Fig. S2 shows pHP1γ immunodetection in PEC of $PTEN^{(i)pe-/-}$ mice. Fig. S3 shows DDR marker immunodetection of in PEC of $PTEN^{(i)pe-/-}$ mice. Fig. S4 shows p53 expression PEC of $PTEN^{(i)pe-/-}$ mice and efficient ablation of p53 in PTEN/$p53^{(i)pe-/-}$ mice. Fig. S5 shows CKIα1, -δ, -γ1, -γ2 and -γ3 transcript levels in the prostate of $PTEN^{(i)pe-/-}$, and control mice at various time points after gene ablation.

Acknowledgments

We thank T. Mak and A. Suzuki for floxed *PTEN* mice and A. Berns for floxed *p53* mice; the staff of the mouse, histopathology, cell sorting, and imaging facilities from Institut de Génétique et de Biologie Moléculaire et Cellulaire and Institut Clinique de la Souris for excellent assistance; P. Kessler and G. Laverny for helpful discussions; and E. Weiss and B. Keyes for critical reading of the manuscript.

This work was supported by funds from the Centre National de la Recherche Scientifique, the Institut National de la Santé et de la Recherche Médicale, the Université de Strasbourg, the Fondation ARC pour la Recherche sur le Cancer, the Ligue Contre le Cancer, Alsace Contre le Cancer, the Association pour la Recherche sur les Tumeurs de la Prostate, the Centre d'Ingénierie Moléculaire Européen, and by French state funds through the Agence Nationale de la Recherche grant ANR-10-LABX-0030-INRT under the frame program Investissements d'Avenir labeled ANR-10-IDEX-0002-02. M. Parisotto was supported by the Association pour la Recherche à l'IGBMC (ARI), E. Grelet by the Ministère de l'enseignement supérieur et de la recherché, R. El Bizri by the Al Bizri Foundation, Y. Dai. by the China Scholarship Council, J. Terzic by the Ecole de l'Institut National de la Santé et de la Recherche Médicale Liliane Bettencourt, and D. Eckert by the Ligue Contre le Cancer.

The authors declare no competing financial interests.

Author contributions: D. Metzger conceived the study together with M. Parisotto; M. Parisotto, E. Grelet, R. El Bizri, Y. Dai, J. Terzic, D. Eckert, L. Gargowitsch, and J.-M. Bonert performed experiments; D. Metzger and M. Parisotto analyzed data and wrote the manuscript.

Submitted: 8 July 2017
Revised: 3 February 2018
Accepted: 10 April 2018

References

Adams, P.D. 2007. Remodeling of chromatin structure in senescent cells and its potential impact on tumor suppression and aging. *Gene.* 397:84–93. https://doi.org/10.1016/j.gene.2007.04.020

Alimonti, A., C. Nardella, Z. Chen, J.G. Clohessy, A. Carracedo, L.C. Trotman, K. Cheng, S. Varmeh, S.C. Kozma, G. Thomas, et al. 2010. A novel type of cellular senescence that can be enhanced in mouse models and human tumor xenografts to suppress prostate tumorigenesis. *J. Clin. Invest.* 120:681–693. https://doi.org/10.1172/JCI40535

Ashcroft, M., R.L. Ludwig, D.B. Woods, T.D. Copeland, H.O. Weber, E.J. MacRae, and K.H. Vousden. 2002. Phosphorylation of HDM2 by Akt. *Oncogene.* 21:1955–1962. https://doi.org/10.1038/sj.onc.1205276

Astle, M.V., K.M. Hannan, P.Y. Ng, R.S. Lee, A.J. George, A.K. Hsu, Y. Haupt, R.D. Hannan, and R.B. Pearson. 2012. AKT induces senescence in human cells via mTORC1 and p53 in the absence of DNA damage: implications for targeting mTOR during malignancy. *Oncogene.* 31:1949–1962. https://doi.org/10.1038/onc.2011.394

Bar, J., N. Lukaschuk, A. Zalcenstein, S. Wilder, R. Seger, and M. Oren. 2005. The PI3K inhibitor LY294002 prevents p53 induction by DNA damage and attenuates chemotherapy-induced apoptosis. *Cell Death Differ.* 12:1578–1587. https://doi.org/10.1038/sj.cdd.4401677

Bartek, J., J. Bartkova, and J. Lukas. 2007. DNA damage signalling guards against activated oncogenes and tumour progression. *Oncogene.* 26:7773–7779. https://doi.org/10.1038/sj.onc.1210881

Bartkova, J., N. Rezaei, M. Liontos, P. Karakaidos, D. Kletsas, N. Issaeva, L.V. Vassiliou, E. Kolettas, K. Niforou, V.C. Zoumpourlis, et al. 2006. Oncogene-induced senescence is part of the tumorigenesis barrier imposed by DNA damage checkpoints. *Nature.* 444:633–637. https://doi.org/10.1038/nature05268

Braig, M., S. Lee, C. Loddenkemper, C. Rudolph, A.H. Peters, B. Schlegelberger, H. Stein, B. Dörken, T. Jenuwein, and C.A. Schmitt. 2005. Oncogene-induced senescence as an initial barrier in lymphoma development. *Nature.* 436:660–665. https://doi.org/10.1038/nature03841

Branzei, D., and M. Foiani. 2005. The DNA damage response during DNA replication. *Curr. Opin. Cell Biol.* 17:568–575. https://doi.org/10.1016/j.ceb.2005.09.003

Byun, T.S., M. Pacek, M.C. Yee, J.C. Walter, and K.A. Cimprich. 2005. Functional uncoupling of MCM helicase and DNA polymerase activities activates the ATR-dependent checkpoint. *Genes Dev.* 19:1040–1052. https://doi.org/10.1101/gad.1301205

Cairns, P., K. Okami, S. Halachmi, N. Halachmi, M. Esteller, J.G. Herman, J. Jen, W.B. Isaacs, G.S. Bova, and D. Sidransky. 1997. Frequent inactivation of PTEN/MMAC1 in primary prostate cancer. *Cancer Res.* 57:4997–5000.

Chen, Z., L.C. Trotman, D. Shaffer, H.K. Lin, Z.A. Dotan, M. Niki, J.A. Koutcher, H.I. Scher, T. Ludwig, W. Gerald, et al. 2005. Crucial role of p53-dependent cellular senescence in suppression of Pten-deficient tumorigenesis. *Nature.* 436:725–730. https://doi.org/10.1038/nature03918

Choucair, K., J. Ejdelman, F. Brimo, A. Aprikian, S. Chevalier, and J. Lapointe. 2012. PTEN genomic deletion predicts prostate cancer recurrence and is associated with low AR expression and transcriptional activity. *BMC Cancer.* 12:543. https://doi.org/10.1186/1471-2407-12-543

Collado, M., and M. Serrano. 2006. The power and the promise of oncogene-induced senescence markers. *Nat. Rev. Cancer.* 6:472–476. https://doi.org/10.1038/nrc1884

Collado, M., and M. Serrano. 2010. Senescence in tumours: evidence from mice and humans. *Nat. Rev. Cancer.* 10:51–57. https://doi.org/10.1038/nrc2772

Cortez, D., S. Guntuku, J. Qin, and S.J. Elledge. 2001. ATR and ATRIP: partners in checkpoint signaling. *Science.* 294:1713–1716. https://doi.org/10.1126/science.1065521

Costa, H.A., M.G. Leitner, M.L. Sos, A. Mavrantoni, A. Rychkova, J.R. Johnson, B.W. Newton, M.C. Yee, F.M. De La Vega, J.M. Ford, et al. 2015. Discovery and functional characterization of a neomorphic PTEN mutation.

Proc. Natl. Acad. Sci. USA. 112:13976–13981. https://doi.org/10.1073/pnas.1422504112

Courtois-Cox, S., S.L. Jones, and K. Cichowski. 2008. Many roads lead to oncogene-induced senescence. *Oncogene.* 27:2801–2809. https://doi.org/10.1038/sj.onc.1210950

Di Micco, R., M. Fumagalli, A. Cicalese, S. Piccinin, P. Gasparini, C. Luise, C. Schurra, M. Garre', P.G. Nuciforo, A. Bensimon, et al. 2006. Oncogene-induced senescence is a DNA damage response triggered by DNA hyper-replication. *Nature.* 444:638–642. https://doi.org/10.1038/nature05327

Di Mitri, D., A. Toso, J.J. Chen, M. Sarti, S. Pinton, T.R. Jost, R. D'Antuono, E. Montani, R. Garcia-Escudero, I. Guccini, et al. 2014. Tumour-infiltrating Gr-1+ myeloid cells antagonize senescence in cancer. *Nature.* 515:134–137. https://doi.org/10.1038/nature13638

Dimri, G.P., X. Lee, G. Basile, M. Acosta, G. Scott, C. Roskelley, E.E. Medrano, M. Linskens, I. Rubelj, O. Pereira-Smith, et al. 1995. A biomarker that identifies senescent human cells in culture and in aging skin in vivo. *Proc. Natl. Acad. Sci. USA.* 92:9363–9367. https://doi.org/10.1073/pnas.92.20.9363

Feng, J., R. Tamaskovic, Z. Yang, D.P. Brazil, A. Merlo, D. Hess, and B.A. Hemmings. 2004. Stabilization of Mdm2 via decreased ubiquitination is mediated by protein kinase B/Akt-dependent phosphorylation. *J. Biol. Chem.* 279:35510–35517. https://doi.org/10.1074/jbc.M404936200

Fenouille, N., A. Puissant, M. Tichet, G. Zimniak, P. Abbe, A. Mallavialle, S. Rocchi, J.P. Ortonne, M. Deckert, R. Ballotti, and S. Tartare-Deckert. 2011. SPARC functions as an anti-stress factor by inactivating p53 through Akt-mediated MDM2 phosphorylation to promote melanoma cell survival. *Oncogene.* 30:4887–4900. https://doi.org/10.1038/onc.2011.198

Ferbeyre, G., E. de Stanchina, E. Querido, N. Baptiste, C. Prives, and S.W. Lowe. 2000. PML is induced by oncogenic ras and promotes premature senescence. *Genes Dev.* 14:2015–2027.

Freeman, D.J., A.G. Li, G. Wei, H.H. Li, N. Kertesz, R. Lesche, A.D. Whale, H. Martinez-Diaz, N. Rozengurt, R.D. Cardiff, et al. 2003. PTEN tumor suppressor regulates p53 protein levels and activity through phosphatase-dependent and -independent mechanisms. *Cancer Cell.* 3:117–130. https://doi.org/10.1016/S1535-6108(03)00021-7

Gali Ramamoorthy, T., G. Laverny, A.I. Schlagowski, J. Zoll, N. Messaddeq, J.M. Bornert, S. Panza, A. Ferry, B. Geny, and D. Metzger. 2015. The transcriptional coregulator PGC-1β controls mitochondrial function and anti-oxidant defence in skeletal muscles. *Nat. Commun.* 6:10210. https://doi.org/10.1038/ncomms10210

Inuzuka, H., A. Tseng, D. Gao, B. Zhai, Q. Zhang, S. Shaik, L. Wan, X.L. Ang, C. Mock, H. Yin, et al. 2010. Phosphorylation by casein kinase I promotes the turnover of the Mdm2 oncoprotein via the SCF(beta-TRCP) ubiquitin ligase. *Cancer Cell.* 18:147–159. https://doi.org/10.1016/j.ccr.2010.06.015

Jonkers, J., R. Meuwissen, H. van der Gulden, H. Peterse, M. van der Valk, and A. Berns. 2001. Synergistic tumor suppressor activity of BRCA2 and p53 in a conditional mouse model for breast cancer. *Nat. Genet.* 29:418–425. https://doi.org/10.1038/ng747

Kang, T.W., T. Yevsa, N. Woller, L. Hoenicke, T. Wuestefeld, D. Dauch, A. Hohmeyer, M. Gereke, R. Rudalska, A. Potapova, et al. 2011. Senescence surveillance of pre-malignant hepatocytes limits liver cancer development. *Nature.* 479:547–551. https://doi.org/10.1038/nature10599

Kim, J.S., C. Lee, C.L. Bonifant, H. Ressom, and T. Waldman. 2007. Activation of p53-dependent growth suppression in human cells by mutations in PTEN or PIK3CA. *Mol. Cell. Biol.* 27:662–677. https://doi.org/10.1128/MCB.00537-06

Knippschild, U., M. Krüger, J. Richter, P. Xu, B. García-Reyes, C. Peifer, J. Halekotte, V. Bakulev, and J. Bischof. 2014. The CK1 Family: Contribution to Cellular Stress Response and Its Role in Carcinogenesis. *Front. Oncol.* 4:96. https://doi.org/10.3389/fonc.2014.00096

Krohn, A., T. Diedler, L. Burkhardt, P.S. Mayer, C. De Silva, M. Meyer-Kornblum, D. Kötschau, P. Tennstedt, J. Huang, C. Gerhäuser, et al. 2012. Genomic deletion of PTEN is associated with tumor progression and early PSA recurrence in ERG fusion-positive and fusion-negative prostate cancer. *Am. J. Pathol.* 181:401–412. https://doi.org/10.1016/j.ajpath.2012.04.026

Lavin, M.F., and N. Gueven. 2006. The complexity of p53 stabilization and activation. *Cell Death Differ.* 13:941–950. https://doi.org/10.1038/sj.cdd.4401925

Liaw, H., D. Lee, and K. Myung. 2011. DNA-PK-dependent RPA2 hyperphosphorylation facilitates DNA repair and suppresses sister chromatid exchange. *PLoS One.* 6:e21424. https://doi.org/10.1371/journal.pone.0021424

Lotan, T.L., B. Gurel, S. Sutcliffe, D. Esopi, W. Liu, J. Xu, J.L. Hicks, B.H. Park, E. Humphreys, A.W. Partin, et al. 2011. PTEN protein loss by immunostaining: analytic validation and prognostic indicator for a high risk surgical cohort of prostate cancer patients. *Clin. Cancer Res.* 17:6563–6573. https://doi.org/10.1158/1078-0432.CCR-11-1244

Luchman, H.A., H. Benediktsson, M.L. Villemaire, A.C. Peterson, and F.R. Jirik. 2008. The pace of prostatic intraepithelial neoplasia development is determined by the timing of Pten tumor suppressor gene excision. *PLoS One.* 3:e3940. https://doi.org/10.1371/journal.pone.0003940

Lukas, C., V. Savic, S. Bekker-Jensen, C. Doil, B. Neumann, R.S. Pedersen, M. Grøfte, K.L. Chan, I.D. Hickson, J. Bartek, and J. Lukas. 2011. 53BP1 nuclear bodies form around DNA lesions generated by mitotic transmission of chromosomes under replication stress. *Nat. Cell Biol.* 13:243–253. https://doi.org/10.1038/ncb2201

Mah, L.J., A. El-Osta, and T.C. Karagiannis. 2010. gammaH2AX: a sensitive molecular marker of DNA damage and repair. *Leukemia.* 24:679–686. https://doi.org/10.1038/leu.2010.6

Mallette, F.A., M.F. Gaumont-Leclerc, and G. Ferbeyre. 2007. The DNA damage signaling pathway is a critical mediator of oncogene-induced senescence. *Genes Dev.* 21:43–48. https://doi.org/10.1101/gad.1487307

Markert, E.K., H. Mizuno, A. Vazquez, and A.J. Levine. 2011. Molecular classification of prostate cancer using curated expression signatures. *Proc. Natl. Acad. Sci. USA.* 108:21276–21281. https://doi.org/10.1073/pnas.1117029108

Mayo, L.D., and D.B. Donner. 2001. A phosphatidylinositol 3-kinase/Akt pathway promotes translocation of Mdm2 from the cytoplasm to the nucleus. *Proc. Natl. Acad. Sci. USA.* 98:11598–11603. https://doi.org/10.1073/pnas.181181198

Mayo, L.D., J.E. Dixon, D.L. Durden, N.K. Tonks, and D.B. Donner. 2002. PTEN protects p53 from Mdm2 and sensitizes cancer cells to chemotherapy. *J. Biol. Chem.* 277:5484–5489. https://doi.org/10.1074/jbc.M108302200

Mazouzi, A., G. Velimezi, and J.I. Loizou. 2014. DNA replication stress: causes, resolution and disease. *Exp. Cell Res.* 329:85–93. https://doi.org/10.1016/j.yexcr.2014.09.030

Meek, D.W. 2009. Tumour suppression by p53: a role for the DNA damage response? *Nat. Rev. Cancer.* 9:714–723. https://doi.org/10.1038/nrc2716

Metzger, D., M. Li, and P. Chambon. 2005. Targeted somatic mutagenesis in the mouse epidermis. *Methods Mol. Biol.* 289:329–340.

Michaloglou, C., L.C. Vredeveld, M.S. Soengas, C. Denoyelle, T. Kuilman, C.M. van der Horst, D.M. Majoor, J.W. Shay, W.J. Mooi, and D.S. Peeper. 2005. BRAFE600-associated senescence-like cell cycle arrest of human naevi. *Nature.* 436:720–724. https://doi.org/10.1038/nature03890

Mirzayans, R., B. Andrais, A. Scott, and D. Murray. 2012. New insights into p53 signaling and cancer cell response to DNA damage: implications for cancer therapy. *J. Biomed. Biotechnol.* 2012:170325. https://doi.org/10.1155/2012/170325

Ogawara, Y., S. Kishishita, T. Obata, Y. Isazawa, T. Suzuki, K. Tanaka, N. Masuyama, and Y. Gotoh. 2002. Akt enhances Mdm2-mediated ubiquitination and degradation of p53. *J. Biol. Chem.* 277:21843–21850. https://doi.org/10.1074/jbc.M109745200

Papa, A., L. Wan, M. Bonora, L. Salmena, M.S. Song, R.M. Hobbs, A. Lunardi, K. Webster, C. Ng, R.H. Newton, et al. 2014. Cancer-associated PTEN mutants act in a dominant-negative manner to suppress PTEN protein function. *Cell.* 157:595–610. https://doi.org/10.1016/j.cell.2014.03.027

Pérez-Mancera, P.A., A.R. Young, and M. Narita. 2014. Inside and out: the activities of senescence in cancer. *Nat. Rev. Cancer.* 14:547–558. https://doi.org/10.1038/nrc3773

Ratnacaram, C.K., M. Teletin, M. Jiang, X. Meng, P. Chambon, and D. Metzger. 2008. Temporally controlled ablation of PTEN in adult mouse prostate epithelium generates a model of invasive prostatic adenocarcinoma. *Proc. Natl. Acad. Sci. USA.* 105:2521–2526. https://doi.org/10.1073/pnas.0712021105

Rodier, F., D.P. Muñoz, R. Teachenor, V. Chu, O. Le, D. Bhaumik, J.P. Coppé, E. Campeau, C.M. Beauséjour, S.H. Kim, et al. 2011. DNA-SCARS: distinct nuclear structures that sustain damage-induced senescence growth arrest and inflammatory cytokine secretion. *J. Cell Sci.* 124:68–81. https://doi.org/10.1242/jcs.071340

Rodriguez, M.S., J.M. Desterro, S. Lain, D.P. Lane, and R.T. Hay. 2000. Multiple C-terminal lysine residues target p53 for ubiquitin-proteasome-mediated degradation. *Mol. Cell. Biol.* 20:8458–8467. https://doi.org/10.1128/MCB.20.22.8458-8467.2000

Rogakou, E.P., D.R. Pilch, A.H. Orr, V.S. Ivanova, and W.M. Bonner. 1998. DNA double-stranded breaks induce histone H2AX phosphorylation on serine 139. *J. Biol. Chem.* 273:5858–5868. https://doi.org/10.1074/jbc.273.10.5858

Schindelin, J., I. Arganda-Carreras, E. Frise, V. Kaynig, M. Longair, T. Pietzsch, S. Preibisch, C. Rueden, S. Saalfeld, B. Schmid, et al. 2012. Fiji: an open-source platform for biological-image analysis. *Nat. Methods.* 9:676–682. https://doi.org/10.1038/nmeth.2019

Serrano, M., and M.A. Blasco. 2001. Putting the stress on senescence. *Curr. Opin. Cell Biol.* 13:748–753. https://doi.org/10.1016/S0955-0674(00)00278-7

Serrano, M., A.W. Lin, M.E. McCurrach, D. Beach, and S.W. Lowe. 1997. Oncogenic ras provokes premature cell senescence associated with accumulation of p53 and p16INK4a. *Cell.* 88:593–602. https://doi.org/10.1016/S0092-8674(00)81902-9

Sirbu, B.M., F.B. Couch, J.T. Feigerle, S. Bhaskara, S.W. Hiebert, and D. Cortez. 2011. Analysis of protein dynamics at active, stalled, and collapsed replication forks. *Genes Dev.* 25:1320–1327. https://doi.org/10.1101/gad.2053211

Vassilev, L.T., B.T. Vu, B. Graves, D. Carvajal, F. Podlaski, Z. Filipovic, N. Kong, U. Kammlott, C. Lukacs, C. Klein, et al. 2004. In vivo activation of the p53 pathway by small-molecule antagonists of MDM2. *Science.* 303:844–848. https://doi.org/10.1126/science.1092472

Vernier, M., V. Bourdeau, M.F. Gaumont-Leclerc, O. Moiseeva, V. Bégin, F. Saad, A.M. Mes-Masson, and G. Ferbeyre. 2011. Regulation of E2Fs and senescence by PML nuclear bodies. *Genes Dev.* 25:41–50. https://doi.org/10.1101/gad.1975111

Ward, I.M., and J. Chen. 2001. Histone H2AX is phosphorylated in an ATR-dependent manner in response to replicational stress. *J. Biol. Chem.* 276:47759–47762. https://doi.org/10.1074/jbc.C100569200

Wei, S., X. Chen, K. McGraw, L. Zhang, R. Komrokji, J. Clark, G. Caceres, D. Billingsley, L. Sokol, J. Lancet, et al. 2013. Lenalidomide promotes p53 degradation by inhibiting MDM2 auto-ubiquitination in myelodysplastic syndrome with chromosome 5q deletion. *Oncogene.* 32:1110–1120. https://doi.org/10.1038/onc.2012.139

Wu, X., J. Wu, J. Huang, W.C. Powell, J. Zhang, R.J. Matusik, F.O. Sangiorgi, R.E. Maxson, H.M. Sucov, and P. Roy-Burman. 2001. Generation of a prostate epithelial cell-specific Cre transgenic mouse model for tissue-specific gene ablation. *Mech. Dev.* 101:61–69. https://doi.org/10.1016/S0925-4773(00)00551-7

Yaswen, P., and J. Campisi. 2007. Oncogene-induced senescence pathways weave an intricate tapestry. *Cell.* 128:233–234. https://doi.org/10.1016/j.cell.2007.01.005

Zhou, B.B., and S.J. Elledge. 2000. The DNA damage response: putting checkpoints in perspective. *Nature.* 408:433–439. https://doi.org/10.1038/35044005

Zhou, B.P., Y. Liao, W. Xia, Y. Zou, B. Spohn, and M.C. Hung. 2001. HER-2/neu induces p53 ubiquitination via Akt-mediated MDM2 phosphorylation. *Nat. Cell Biol.* 3:973–982. https://doi.org/10.1038/ncb1101-973